Patient-specific biokinetics and hybrid 2D/3D approach integration in OEDIPE software: application to radioiodine therapy

Mohammed Bensiali, Nadège Anizan, Sophie Leboulleux, Stephanie Lamart, Estelle Davesne, David Broggio, Aurelie Desbree, Didier Franck

Patient-specific biokinetics and hybrid 2D/3D approach integration in OEDIPE software: application to radioiodine therapy

M. Bensiali [1], N. Anizan [2,4], S. Leboulleux[4,5], S. Lamart[1*], E. Davesne [1,3], D. Broggio[1], A. Desbrée [1], D. Franck[1]

[1] Laboratoire d'Évaluation de la Dose Interne, Institut de Radioprotection et de Sûreté Nucléaire, IRSN/PSE-SANTE/SDOS/LEDI, Fontenay-aux-Roses, France

[2] Gustave Roussy and University Paris Saclay, Medical Physics Department, Villejuif, France

[3] INSTN, Laboratoire Radioprotection et Santé, Gif-sur-Yvette, France

[4] Gustave Roussy and University Paris Saclay, Nuclear Medicine Department, Villejuif, France

[5] Present address: Department of Endocrinology, Diabetes, Nutrition and Therapeutic Patient Education, Geneva University Hospitals, Geneva, Switzerland

***Corresponding author**: Stephanie Lamart.

Email: stephanie.lamart@irsn.fr

Abstract

Background The development of targeted radionuclide therapy requires the development of dosimetry software accounting for patient-specific biokinetics. New functionalities were thus developed in the OEDIPE software, to deal with multiple 3D images or multiple planar images and a SPECT image. **Materiel & Method** Methods were implemented to recover patient biokinetics in volumes of interest. If several 3D SPECT images are available, they are registered to a reference CT scan. When several planar images and a single SPECT are available, the planar images are registered to the SPECT and counts of the planar images converted to activity. To validate these developments, six SPECT/CT and planar images of a Jaszczak phantom containing I-131 were acquired at different dates. Cumulated activity was estimated in each sphere using the SPECT/CT images only or the planar series associated to one SPECT/CT. Biokinetic and doses in lesions and in the lungs of a patient treated with I-131 for differentiated thyroid cancer were then estimated using four planar images and a SPECT/CT scan. Whole-body retention data were used to compare the biokinetics obtained from the planar and SPECT data. **Results** Activities and cumulated activities estimated using OEDIPE in the phantom spheres agreed well with the reference values for both approaches. Results obtained for the patient compared well with those derived from whole-body retention data. **Conclusion** The implemented features allow automatic evaluation of patient-specific biokinetics from different series of patient images, enabling patient-specific dosimetry without the need for external software to estimate the cumulated activities in different VOIs.

Keywords: radiopharmaceutical therapy (RPT); patient-specific biokinetics; internal dosimetry; multimodal imaging; lesion dosimetry

1. Introduction

Targeted radionuclide therapy (TRT) has demonstrated its clinical efficacy in treating malignant or begin thyroid disease with iodine-131 (I-131) [1-3]. In addition to I-131, Y-90 microspheres are increasingly used for the treatment of liver cancers, as well as Lu-177 coupled with different tumour-specific vectors [4]. The clinical application of TRT with I-131 is commonly based on the administration of a fixed activity, regardless of the patient-specific biokinetics of the radiopharmaceutical, which could lead to an underdose preventing tumor control, or an overdose that may induce toxicity to the organs at risk [5]. However, as recalled in [6], the European Council Directive 2013/59 requires that therapeutic exposure, including nuclear medicine treatment, shall be individually planned, even though improvement of the treatment efficacy have not been proven with the existing models yet [7].

Obtaining the patient-specific biokinetics requires the measurement of the activity present in tissues at several time points after the radiopharmaceutical administration. For that purpose, volumes of interest (VOIs) are analyzed on Nuclear Medicine (NM) images. These images can be series of positron emission tomography (PET) or single-photon emission tomography (SPECT) 3D images, series of 2D images from planar scintigraphy [8], or a series of planar images associated with a single SPECT/CT [9, 10], the so-called hybrid approach. Because the acquisition time of a planar image is much shorter than that of PET or SPECT images, a series of planar images may be obtained more easily in clinical practice than a series of 3D images. However, fixations from different lesions and/or tissues may result in overlapping source regions on the planar image, which makes activity quantification difficult and can lead to additional sources of uncertainty in absorbed dose estimates [11]. In the hybrid approach that combines a series of planar images with a 3D image, activity quantification is based on the 3D

image and is hence expected to be better than when solely based on planar images, because attenuation correction, scatter correction and detector response are more precisely determined. Biokinetics is still based on planar images. Thus, overlapping source regions remains an issue and it may be challenging to define a one-to-one correspondence between 2D regions and 3D contours from the 3D image. Fully 3D dosimetry appears to be the method of choice in terms of activity and biokinetic quantification but it remains difficult to acquire series of 3D images in clinical practice [12, 13]. Regardless of the method used for the obtention of time-activity data-points, numerical and/or analytical time integration of image-based time activity curves (TACs) is performed to derive the cumulated activity in tissues that are used for the computation of the tissue absorbed doses.

Different approaches can be adopted to convert the cumulated activities into absorbed doses. The first one, which disregards patient-specific anatomy, consists in applying pre-calculated S factors, obtained from reference computational models [14]. The second approach consists in using the convolution of dose voxel kernels (DVK), [15, 16]. DVK methods account for the patient-specific anatomy and for the activity heterogeneity with a calculation time that remains reasonable [17]. However, the DVK methods do not enable modeling the density heterogeneity within VOIs [18] and DVK must be pre-calculated using Monte Carlo radiation transport code [19]. The third approach consists in using Monte Carlo calculation, taking into account the patient-specific anatomy [20, 21]. Considering the patient specific anatomy, tissue heterogeneity and activity distribution can result in relatively time-consuming Monte Carlo calculations compared with the two aforementioned methods.

Many in-house or commercial software have been developed to enable treatment planning in nuclear medicine [12, 22, 23]. Some of them, such as STRATOS (Philips Technologie, Aachen,

Germany) [24] or PLANET® Onco Dose (DOSIsoft, Cachan, France) [25] allow combined analysis of 3D and 2D images.

Some examples of dosimetry studies taking advantage of the hybrid approach have been reported recently. In [26], Lu-PSMA-617 time-activity curves were obtained from 2D and 3D SPECT images using the QDOSE software, but dosimetry was performed with IDAC-Dose2.1. This software enables calculation of organ absorbed doses from cumulated activities based on organ S values pre-calculated on reference voxel phantoms [27]. In [28], pre-therapeutic imaging with In-111 was performed for patients treated with Y-90 ibritumomab tiuxetan ; 2D and 3D SPECT images were acquired and quantified and then doses calculated with MIRDose 3.0. Similarly, in [29], hybrid images were quantified and then doses calculated with pre-calculated S-factors in order to asses bone marrow doses following 177Lu-DOTATATE therapy. Finally, Kupitz and colleagues [30] have used the dosimetry toolkit from GE Healthcare to acquire, register and quantify hybrid images following Lu-177-DOTATATE therapy, doses were then calculated with OLINDA/EXM, which uses reference organ S values [14].

The OEDIPE software has been continuously developed at the French Institute for Radiation Protection and Nuclear Safety (IRSN) and applied to carry out personalized 3D dosimetry in nuclear medicine using Monte Carlo simulation [31, 32]. Developments had been initiated in OEDIPE to derive biokinetics from SPECT/CT and PET/CT images [33]. However, series of 3D images are not always available in the clinical practice, whereas it is more feasible to acquire planar images at several time-points. Therefore, new functionalities have been implemented to handle a hybrid approach that uses a series of planar images in association with a SPECT/CT image.

The implementation of the features enabling registration, quantification and derivation of TAC from multiple 3D or hybrid image data is presented. These developments were validated using measurements carried out with a Jaszczak phantom filled with I-131 (Cylindrical Jaszczak phantom, Data Spectrum, Durham, NC, USA). The hybrid dosimetry approach is then applied to the case of a thyroid metastatic patient treated with I-131. The biokinetics of I-131 in the lungs and metastases, obtained from the hybrid-approach, are compared and validated with external dose rate measurements. Because lesions are generally characterized by relatively small volumes [34] and because their dose assessment remains still challenging [35], we address the issue of small volumes in the phantom experiment and patient case.

2. MATERIAL AND METHODS

After a brief description of the previous version of OEDIPE software, the new functionalities will be described, as well as the methods used for the validation of the developments.

2.1. OEDIPE software

Patient's anatomical data can be imported in OEDIPE as CT or MRI images. VOIs are defined by threshold-based segmentation on image values. VOIs can also be directly imported as DICOM RT-structure file, generated from contours delineated using external software such as PLANET® Onco Dose (DOSIsoft, Cachan, France). A voxelized phantom of the patient is subsequently generated and the user defines the composition and densities of VOIs. Functional images are imported as SPECT or PET images associated with a CT exam. The cumulated activity in the voxel phantom can be distributed either homogeneously within selected VOIs or heterogeneously through the phantom according to the quantitative emission data available in input. In this case, each voxel is assigned a fraction of the cumulated activity derived from a single functional image. The source spatial distribution can be associated to one of the 246 radionuclides available, with emission spectra taken from ICRP

publication 38 [36]. Hence, the patient's treatment with a radiopharmaceutical can be fully modelled using OEDIPE (anatomy, material, density, cumulated activity distribution of the radionuclide). OEDIPE subsequently enables automatic transcription of this model into an input file for MCNPX Monte-Carlo code [37]. MCNPX may directly compute mean absorbed doses or a dose-rate map used in OEDIPE to provide mean absorbed doses, biological effective doses, iso-dose maps and dose-volumes histograms for the selected VOIs. Figure 1 shows the flow of input and output data involved in the OEDIPE environment.

2.2. New features: patient-specific biokinetics from multiple functional images

As different types of NM images may be available in clinical practice, two processes of image analysis were implemented to retrieve activity from either the fully 3D and/or the hybrid approach. In addition, a biokinetic module was implemented to calculate the cumulated activity in VOIs based on the output of both image analysis processes.

2.2.1. Analysis process for multiple 3D NM images

It is first necessary to register 3D functional images to a reference anatomical image before retrieving activities in VOIs. The reference anatomical image, called thereafter $CT_{REFERENCE}$ is used to generate the voxel phantom.

Registration is rigid and performed manually on a specific graphical interface. It is possible to either register the 3D NM images directly to the reference CT (SPECT-$CT_{REFERENCE}$ registration). Because NM images are usually already registered to a CT scan, it is also possible to register this CT image to the $CT_{REFERENCE}$ (CT-$CT_{REFERENCE}$ registration), embarking the NM image in the process. Whatever the choice, the functional images are resampled to the resolution of the reference image. This registration interface was already available [32] but was limited to

register a single image only. Currently, this interface is subsequently called for every 3D NM image that needs to be registered for the present implementations.

After registration, in each emission image, the sum of counts in each selected VOIs is computed. To convert these counts into activity, the same calibration factor can be applied to all 3D NM images or an image-specific one can be assigned to each image. The second option is particularly useful to correct images for dead-time effect or when images have not been acquired with the same camera [38] and/or different acquisition/reconstruction parameters were used. Conversion of counts into activity considered the quantitative SPECT data decay corrected at the time of the radiopharmaceutical administration. Once the processing of the 3D NM images is completed, the time and activity data for each VOI are transferred to the biokinetic module (see 2.2.3).

2.2.2. Analysis process for multiple planar-single SPECT images (hybrid)

In the hybrid approach, the SPECT/CT must be first processed as described above. Then, planar images can be imported, registered and quantified.

Manual registration can be carried out either onto the 2D projections of the VOIs using anterior or posterior views ($VOIs_{PROJECTION}$ in **Figure 1**), or onto the 2D projections of the SPECT image ($SPECT_{PROJECTION,}$ **Figure 1** and **Figure 2**). This option enables visualization of the superimposition of counts distributions: regions of high fixation present in both images are helpful markers for precise registration. As for 3D image registration, 2D images are resampled to the resolution of the reference image.

After registration, sum of counts in registered planar images are extracted in each VOI, using the anterior and posterior views, and their geometric mean is calculated. The geometric mean is converted to activities in each VOI using a 2D/3D conversion factor $\left(\boldsymbol{f_{2D/3D}}\right)_{\boldsymbol{VOI}}$. This factor

is calculated from the SPECT activities and the count number of the planar image, which was acquired just before or after the SPECT image:

$$\left(f_{2D/3D}\right)_{VOI} = \frac{A_{VOI-3D}}{C_{VOI-2D}(t_{SPECT})} . \Delta t$$

Equation 1

Where,

$C_{VOI-2D}(t_{SPECT})$ is the geometric mean of counts in the planar image acquired at t = t_{SPECT} and associated to a given VOI,

Δt is the acquisition duration of the planar image (s),

A_{VOI-3D} is the VOI activity determined from the SPECT (MBq).

Conversion of the geometric mean of counts from planar images into activity at successive time points is obtained as follows:

$$A_{VOI}(t) = \frac{C_{VOI-2D}(t)}{\Delta t'} . \left(f_{2D/3D}\right)_{VOI}$$

Equation 2

Where $\Delta t'$ is the acquisition duration of the planar image (s)

Once the activity in the considered VOIs is computed for each acquired image time point, time activity data are transferred to the biokinetic module and managed as described in the next paragraph.

2.2.3. Biokinetic module

The purpose of this module is to estimate the cumulated activity in each VOI from the time-activity data. In order to account for a possible partial volume effect [39], a recovery

coefficient, R_{VOI}, can be applied for each VOI. The corrected activities $[\boldsymbol{A_{VOI}(t)}]_{\boldsymbol{R}}$ are then calculated as:

$$[\boldsymbol{A_{VOI}(t)}]_{\boldsymbol{R}} = \frac{\boldsymbol{A_{VOI}(t)}}{\boldsymbol{R_{VOI}}}$$

Equation 3

The cumulated activity is calculated at the VOI level and it consists in integrating the time-activity curve (TAC) from the time of administration to complete elimination. The TAC is divided into three intervals:

(i) the pre-maximum interval: period from the administration time to the time when the activity in the VOI is maximal,

(ii) the central interval: from the end of the previous interval to the time of the last acquired image,

(iii) the final interval: from the acquisition time of the last image time to infinity.

The shape of the TAC during the pre-maximum interval depends on the selected initial conditions. If the activity at the time of administration is assumed to be null, the TAC is a line that passes through the origin and the highest point. Otherwise, the function chosen for the central interval is extrapolated back to the injection time (t=0).

For the central interval the shape of the TAC can be mono-exponential, bi-exponential, or a piecewise linear function. The parameters of the exponential functions are computed by a non-linear least squares regression.

The TAC on the final interval is calculated as the extrapolation of the TAC determined on the central interval. **Figure S.1** (Supplementary Material) shows the biokinetic module: among other parameters, cumulated activity, relative cumulated activity and the chi-square are

displayed. In addition to the chi-square value as an indication of the goodness-of-fit, the effective half-life is provided, which enables the user to verify whether its value is smaller than the physical half-life of the radionuclide. The resulting cumulated activities may be distributed according to a 3D image, in proportion of the counts in the image voxels.

2.3. Validation of the developments with phantom data

2.3.1. Phantom data acquisition

Images of a Jaszczak phantom were used to validate the new functionalities (Cylindrical Jaszczak phantom, Data Spectrum, Durham, NC, USA). Each sphere of the Jaszczak phantom (0.5 ml to 16 ml) was filled with a 9.36 MBq/mL solution of I-131. The total activity in the phantom was hence 294.7 MBq. The phantom contained no background so that the validation results could be interpreted with a minimum of artefacts. Six SPECT/CT images were acquired with a GE Discovery NM/CT 670 gamma camera at 4, 7, 11, 14, 18 and 22 days post-injection (see **Figure S.2** in Supplemental Material). After each SPECT/CT acquisition, a planar image was acquired with the phantom in the same position.

The SPECT acquisition was performed using the parameters summarized in **Table 1**. SPECT reconstructions were carried out using Xeleris 3.1 software (GE) using OSEM (the Ordered Subset Expectation Maximization) that included CT-based attenuation correction and dual energy window scatter correction, with 2 iterations, 10 subsets, and a Butterworth filter of 0.48 and a cutoff of 10.

The acquired images were used to validate the implementation of the methods developed for TAC derivation: the multi-SPECT approach using SPECT/CT images only (2.2.1) and the hybrid approach (2.2.2), respectively.

Table 1. Acquisition parameters of the SPECT images.

Collimator	HEGP
Photopeak window	364 keV ± 10%
Scatter window	297 keV ± 10%
SPECT movement	Body contour
Matrix	128x128
Projections	2x30 projections
Time per projection	25 s

2.3.2. Multi-SPECT approach

A voxel phantom of the Jaszczak phantom was created after delineation of the spheres (VOIs) and of the outside contour on the CT of the first SPECT image. Delineation was carried out with PLANET® Onco Dose (PDOSE) software from DOSIsoft (Cachan, France). As described in *2.2.1*, a CT-$CT_{REFERENCE}$ registration was carried out. The calibration factor was obtained using the same phantom, acquisition and reconstruction parameters as described in 2.3.1., and was used as an input parameter in OEDIPE (25.5 counts.s-1.MBq-1). Recovery factors, as a function the object size, were obtained from the Jaszczak experiment and entered in the software to correct for the partial volume effects and improve the quantitative accuracy of the dosimetry workflow (see **Table S.1** in Supplementary Material**)**. A mono-exponential model was used to fit the time-activity curve (TAC) for each VOI, and to estimate cumulated activities.

The obtained time-activity values were compared with the known values derived from the radioactive decay of I-131, characterized by a physical half-life of 8.02 days. To evaluate the accuracy of calculated cumulated activity ($\tilde{A}_{OEDIPE}$), the percentage difference with the known values ($\tilde{A}_{Known}$) was computed:

$$100 - \%Difference = 100 \times (1 - \frac{\tilde{A}_{OEDIPE} - \tilde{A}_{Known}}{\tilde{A}_{Known}})$$

Equation 4

2.3.3. Planar-SPECT approach

Six associations of multiple planar and one single SPECT images were studied: the planar images were associated with one of the six SPECTs to convert planar count rates to activities. These associations are hereafter referred to as Planar + SPECT_i. The same voxelized phantom created for the multi-SPECT approach was used. As described in *2.2.3* the projection of the SPECT was used to register the planar images. To obtain the $f_{2D/3D}$ factor, the activity in the VOI (cf. Eq. 1) was obtained using the same calibration and recovery factors as in the multi-SPECT approach. The mono-exponential model was chosen to fit the time-activity curve (TAC) for each VOI, and to estimate cumulated activities. Like in the multi-SPECT approach, time-activities in each VOI were compared with the expected values as well as the cumulated activities.

2.4. Application to a patient case

The implemented processing of hybrid images was applied to a patient case as an ancillary study of the multicentric prospective MERAIODE study [40]. The patient suffering from a *BRAF* mutated radioiodine refractory metastatic differentiated thyroid cancer, was injected with 5.74 GBq of I-131, following recombinant human TSH injections after 5 weeks of treatment with dabrafenib and trametinib drugs to reinitiate iodine uptake. One SPECT/CT and planar images were used to estimate the biokinetic and doses of the lungs and of six lung tumors. For this patient, whole body dose rate measurements were also available.

2.4.1. Imaging data

Four planar whole-body images and a SPECT/CT were acquired **(Figure 3)**. The planar images (256×1024 pixels), were acquired with a GE Discovery NM/CT 670 equipped with a HEGP collimator, at 23.7, 43.5, 65.3 and 88 hours after the radioiodine administration. The SPECT/CT scan was acquired a few minutes after the last planar imaging using the same gamma camera. The SPECT acquisition and reconstruction parameters are the same as those used to acquire images of the Jaszczak phantom.

VOIs contours were outlined manually using the PDOSE software by an experienced physician on a diagnostic CT image, acquired few days before the radioiodine treatment. The VOIs and the corresponding contour characteristics are listed in Table 2.

Table 2: Characteristics of the volumes of interest (VOI). L: left, R: right.

VOI	Location	Volume (ml)	I-131 activity from quantitative SPECT/CT (MBq)
Lungs	**Lungs**	**4 445**	**528.15**
Lesion 1	**Para tracheal lymph node**	**0.26**	**12.03**
Lesion 2	**Lung L**	**0.23**	**15.85**
Lesion 3	**Lung R**	**1.02**	**18.65**
Lesion 4	**Lung L**	**0.78**	**19.31**
Lesion 5	**Lung R**	**1.34**	**22.04**
Lesion 6	**Lung R**	**0.89**	**32.35**

2.4.2. Determination of the time-activity curves, cumulated activities and doses

From the contours delineated with PDOSE a voxel phantom with a size of 256×256×577 was generated. A density of 1.04 g/cm^3 was assigned to soft tissues and lesions, and 0.296 g/cm^3 to the lungs [41]. The quantification of the lesions and lungs activities on the SPECT/CT images were based on the calibration factor derived from the previous Jaszczak phantom measurements. The activities are reported in **Table 2**. For planar images, dead-time correction

factors were assessed using repeated acquisitions of a cylindrical source with a high initial activity in I-131 (3900 MBq), located in a large elliptical physical phantom. Repeated whole-body scans, with the same acquisition protocol as the one used for patients, were carried out during the radioactive decay of the source up to a remaining activity of 590 MBq. Dead-time correction factors were estimated by adjusting a non-paralyzable model to measurement results. The obtained values were 1.5, 1.35 and 1.15 for the three first planar images, respectively. The SPECT anterior-posterior projection was used for the registration of planar images. Tracheal lesion (lesion-1) was used as a registration marker for all planar images because it was the brightest VOI in both image types. Then counts in VOIs were converted to activities using Equation 1. A mono-exponential function was used to fit the time-activity curves of each VOI. The correlation coefficient (R^2) was calculated to assess the goodness of fit. The homogeneous distribution option was selected to distribute the cumulated activities and to compute mean absorbed doses. The cumulated activities were distributed in all sources (i.e., the 6 tumors and the lungs) to compute doses using a single calculation. The number of starting particles in MCNPX was 300 000.

2.4.3. Exploitation of whole-body dose rate measurements

Eight measurements of the whole-body retention were acquired using a NaI(Tl) scintillator (Ludlum PM Model 44-2, Ludlum Measurements, Inc., Sweetwater, TX, USA) during the time interval from the first and the last planar image acquisitions (see **Figure S.3** in Supplementary Material). This detector is installed in the ceiling space of the patient's room above the bed. Every acquisition is signaled beforehand by an audible alarm so that the patient returns to a supine position on the bed. Because whole-body retention was measured after the rapid phase of I-131 elimination, the effective half-life of the whole-body retention ($\boldsymbol{T_{whole-body}}$) was determined by fitting a mono-exponential model to the 8 measurements. First, this

effective half-life can be compared with the one obtained from the biokinetic derived from SPECT images processing. Second, one can derive an approximation of the cumulated activities in VOIs.

For that purpose, we simply assumed a mono-exponential decrease of the activities in VOIs with $\boldsymbol{T_{whole-body}}$. We considered the activity at the time of the SPECT/CT image is the one given in Table 2 and deduced the cumulated activity:

$$\widetilde{A}_{VOI} = \frac{A_{VOI-SPECT} \cdot T_{whole-body}}{\ln 2 \,.\, e^{-\frac{\ln 2}{T_{whole-body}} \cdot t_{SPECT}}}$$

Equation 5

The cumulated activities estimated by this approach were distributed homogeneously in the different VOIs and the same dose calculation was performed as above.

3. Results

3.1. Validation with phantom data

3.1.1. Multi-SPECT approach

Figure 4 shows the TACs obtained with the multi-SPECT approach for the spheres of 8, 2 and 0.5 mL of the Jaszczak phantom. Reference curves based on the initially filled activity and physical decay are included. Data for the three other spheres are shown in **Figure S.4** (Supplementary Material).

The median error on the estimated activity, all time points considered, was less than 13% for all spheres. The smallest relative difference between the estimated activity and the theoretical activities were for the largest sphere of 16 mL and were ranging from 0.6% to 18%, whereas the highest relative differences were for the smallest sphere (from -16.7% to 23.4%). The

relative difference ranged between -10% and 20% for the other spheres. The most significant relative differences for all spheres were obtained for the last SPECT acquisition, for which remaining activities in the spheres were the smallest ranging from 0.6 MBq to 20 MBq.

Integrating the TACs, the cumulated activities were obtained. The comparison of known cumulated activities and those assessed is reported as 100-Percentage% in **Figure 5** (left). The relative difference on the estimated cumulated activity was less than 9% for all spheres.

3.1.2. Planar-SPECT approach

Figure 6 shows the time-activity data obtained with the planar-SPECT approach considering the six possible combinations (Planar + SPECT_i). **Figure 6** shows the data for the spheres of 8, 2 and 0.5 mL, data for the three other spheres are given in **Figure S.5** (Supplementary material). Both figures show the theoretical TACs deduced from the initial activities.

The percent difference between the estimated activities depended on the SPECT images selected for the calculation of the $f_{2D/3D}$ factor and increased as the volume of the sphere decreased. For example, the relative difference in activities ranged from -5% to +6% for sphere 1 (16 mL), whereas it varied from -16% to +11% for sphere 5 (1 mL). The greatest errors were obtained for the smallest sphere, i.e., from -27% to +33%. Besides, the selection of SPECT_6, for which the activity was the lowest as compared with the previous time points, resulted in the greatest relative differences.

The comparison of the estimated cumulated activities with the known values is reported as 100-Percentage% in **Figure 5** (right). The relative difference increased with decreasing sphere volumes, regardless of the SPECT selected for activity quantification. The relative difference ranged between ± 5% for sphere 1 (16 mL) and ± 20% for sphere 5 (1 mL). For sphere 6 (0.5 mL), the relative difference varied between -37% and 45%.

3.2. Application to a patient case

3.2.1. Determination of time-activity curves (TACs)

The time-activity data and exponential TACs obtained with the planar-SPECT approach are shown on **Figure 7** along with the R^2 values of the fit. The effective half-life for these curves ranged from 46.1 h (lesion 2) to 79.4 (lesion 5), as reported in **Table 3**. The mono-exponential fit of the time-activity data resulted in R^2 values between 0.821 (lesion 5) and 0.986 (lesion 6).

The effective half-life deduced from whole-body measurements was 65.1 hours. The corresponding TACs are also shown in **Figure 7**. A relative difference of 7.2% in half-life was observed for the lungs between the method based on whole-body retention data and the hybrid approach. For lesions, the difference ranged from -41% (lesion 2) to 18% (lesion 5).

Across times of planar acquisition, the relative difference in lung activities between the two methods was smaller than 13 %. For lesions, the differences ranged from 6% to 17% for lesion 1, from 30 % to 50 % for lesion 2, from -2 % to 25 % for lesions with a volume between 0.5 mL and 1 mL (lesions 4 and 6), and from -13 % to 12% for lesions with a volume greater than 1 mL (lesions 3 and 5).

3.2.2. Estimation of the cumulated activities and doses

The cumulated activities deduced from the planar-SPECT and WB-SPECT methods are reported in **Table 3**. The cumulated activities were systematically higher for the planar-SPECT method. For the lungs, the two methods agreed within 3%. For the lesions, the cumulated activities were between 2.9 and 7.9 GBq.h, the relative differences between the two assessment methods ranged from 2% (lesion 1 and 6) to 12% (lesion 2).

The doses obtained from the cumulated activities and Monte-Carlo calculations are reported in **Table 3**. For lesions, they ranged from about 400 Gy (lesion 5, WB-SPECT method) to 1 900 Gy (lesion 2, planar-SPECT method). Absorbed doses to lungs were about 10 Gy. The relative differences in doses between the two approaches are exactly the same as for the cumulated activities. The computational uncertainties on doses ranged between 0.4% (lesion 3 and 4) and 6% (lesion 1).

Table 3. Effective half-life, cumulated activity and Monte Carlo based estimates of absorbed doses obtained with the hybrid and whole-body (WB) methods.

		Lesion 1	Lesion 2	Lesion 3	Lesion 4	Lesion 5	Lesion 6	Lungs
Effective half-live (hrs)	Planar-SPECT	56.4	46.1	74.9	64.4	79.4	58.3	60.7
	WB	65.1	65.1	65.1	65.1	65.1	65.1	65.1
Cumulated Activity (MBq.h)	Planar-SPECT	2.95E3	4.32E3	4.71E3	5.06E3	5.91E3	7.92E3	1.11E5
	WB	2.88E3	3.80E3	4.47E3	4.63E3	5.28E3	7.76E3	1.08E5
Dose (Gy)	Planar-SPECT	1117	1858	475	663	453	906	10.7
	WB	1092	1635	451	606	405	888	10.4

4. Discussion

4.1. Validation of the multi-SPECT approach

Time-activity data results from different contributions. For instance, parameters and corrections applied in the image reconstruction process, methods used for quantitative calibration, presence of partial volume effect and method applied for its correction [42], [43]. The major source of error potentially introduced during the validation of the multi-SPECT approach resides in the image registration. To validate the implemented functionality, the

phantom experiment was carried out without background activity so that the only possible bias was registration errors.

The percent errors, obtained with the multi-SPECT approach, on the determination of I-131 activity in the Jaszczak phantom spheres, can be compared with the results reported in [38], where for a sphere of 5 cm in diameter (65 mL) the quantification bias was of the order of 16%. Here, the quantification error was less than 20% for the 4 mL sphere.

4.2. Validation of the planar-SPECT approach

We estimated relative percent difference of cumulated activities for each of the spherical insert present in the phantom. In the phantom experiment, we found higher percent difference values when applying the hybrid approach as compared with the multi-SPECT one. This difference can be explained by the error introduced by the registration step on the number of estimated counts. In the fully 3D approach, we used CT-$CT_{REFERENCE}$ registration, which minimizes the error on the estimated numbers of counts from the different 3D images regardless of the volume of the spheres. On the contrary, in the hybrid approach, we registered the projection of the reference SPECT to each planar image, which introduced a much greater error on the estimated number of counts from planar images. In addition, the conversion factor ($f_{2D/3D}$) is also subject to an error induced by the reference registration. Moreover, this error increases as the volume decreases because of the poor resolution of scintigraphic images. As a result, the estimated numbers of counts from the series of planar images may not follow a smooth exponential decrease in the hybrid approach, especially for small volumes, which may lead to greater errors on the estimated cumulated activity. However, these results are consistent with those cited in MIRD no. 23 [44], where the absorbed dose determined using a planar-SPECT method in two lesions with volumes of 5 mL

led to relative percent differences from -10% to 56%, whereas the percent difference in the cumulated activity obtained in the presented OEDIPE analysis varied within ± 20% for the sphere of 4 mL.

The results of the planar-SPECT approach also showed that the choice of the time of the SPECT acquisition after injection can strongly influence the results obtained by this approach as the volume decreases. From our results, it seems that choosing the reference SPECT in the middle of the time interval minimizes the error on the estimated cumulated activity. It could be explained by the fact that the reference SPECT projection used to register planar images is a "median image" capturing well the low or high counting statistics of temporal adjacent planar images. This hypothesis might be of more practical interest in a patient case where organs and tissues are subject to their own biokinetics. If only one SPECT can be acquired, it might be relevant to acquire it in the middle of the time interval of planar images, when the SPECT potentially captures the "median" spatial distribution of activity.

It was also shown, as expected, that the error on time-activity or cumulated activity increased with decreasing volumes. Consequently, dose uncertainties should be relatively large for the smallest tumors.

4.3. Application to a patient case

4.3.1. Assessed tumour half-lives and doses

As recalled in [45], there is no clear consensus regarding the optimal dosage of radioiodine therapeutic activity when treating metastatic disease ; there is only a small number of studies reporting quantitative data on lesions biokinetics and dosimetry. Still, some studies reported such data for patients preliminary treated with rhTSH. In [46], for patients having lung or bone metastases, the mean effective half-life of I-131, was 29 h (range 5.6-129 h). The effective

half-life varied from 9 to 36 hours across 7 lung tumours in [47] and from 34 to 140 hours (16 lung tumors) in [48]. In [49], the effective half-life in thyroid remnants was studied for 33 individuals subject to prior rhTSH simulation, and the half-life was 68 ± 49 h, whereas in [50] the effective half-life in thyroid remnants was 10.5 h in 36 individuals treated after rhTSH simulation, and 15.7 h in 218 individuals treated after thyroid hormone withdrawal. The effective half-lives estimated in the present work for the patient are thus comparable with the data reported in the literature characterized by a wide range of values.

Only a few studies reported doses in metastases. Wierts and colleagues [51] considered 47 patients administered with 5.6 GBq of I-131, with and without rhTSH simulation, and assessed doses to 45 metastases. The doses ranged between a few grays and a few thousand grays with a median around 400 Gy for responding tumours. In [52] a dosimetry study was performed for a pediatric patient suffering from extensive lung metastases. The tumor dose was found to be 64 Gy for 1.7 GBq of administered radioiodine. In [53] the dose to 56 tumors from 15 patients were analyzed and the tumor doses ranged from 0.08 to 49 Gy/GBq. The tumor doses assessed for our patient case ranged from 73 to 330 Gy/GBq and are thus comparable with the literature data. In this work, small tumor volume and relatively long effective half-lives might have resulted in relatively high tumor doses. The uncertainty on the tumor doses and the correlation between doses and tumor response are beyond the scope of this study. Among the multiple sources of uncertainties affecting activity assessment, the background contribution, affecting the recovery factors, has not been considered. However, it was estimated that the signal to background ratio (lesion activity over surrounding healthy lung activity) was between 5 and 10 and thus should not considerably affect the activity assessment. Still, the relatively large errors found on cumulated activities with the smallest sphere of the phantom indicates that they could be as large as 40%.

4.3.2. Comparison of planar-SPECT and WB-SPECT approaches

External dose rate measurements of patients suffering for differentiated thyroid cancer of different grades was reported in [54]. The WB effective half-life ranged between 4 and 56h, it was on average longer for patients having metastases.

The planar-SPECT and WB-SPECT approaches showed consistency of results. These results hence indicate that, when multiple patient images are not available, external total body dose rate measurements might be used for personalized lesion dosimetry. Using an external detector located in the patient's room presents advantages over serial acquisitions of planar images because it enables decreasing the radiation exposure of practitioners, improves patient comfort and decreases gamma-camera occupancy. Therefore, it would be interesting to investigate further this approach on several patients to be able to conclude on its reliability and limitations.

4.4. Further remarks

4.4.1. Study limitations

The implemented method for SPECT registration to a reference CT image or planar registration to a projected SPECT has been tested thanks to a single phantom experiment with one radionuclide. However, the implemented algorithm is rather simple since it relies on manual registration. Further tests in more complex situations (e.g., when background activity is present) might give insights on the limitation of the method but would not question the implemented feature itself.

Currently, the activity assessment in OEDIPE relies on the calibration factors provided by the user or included in the DICOM images. No special module is devoted to their assessment.

Similarly, OEDIPE processes images in DICOM format and thus depends on the reconstruction parameters implemented in the imaging device. Processing of raw data is not possible.

The application to actual patient data demonstrates that the implemented features are applicable in the clinical practice. Although the estimated effective half-lives and doses are comparable with literature data, these results cannot be extrapolated to other patients.

4.4.2. Usefulness of Monte-Carlo calculations

To facilitate comparison with known data, we aimed first at addressing simple experimental and clinical conditions related to radioiodine therapy. For such a short-range emitter, full Monte-Carlo calculations are not strictly necessary.

Still, the MCNPX calculation time to assess mean doses in the patient case was 65 mins, which is compatible with clinical applications. OEDIPE software can be run on a regular PC or laptop. In this work, MCNPX calculations were run on a dedicated cluster. Each calculation was launched on a single node, characterized by 2 CPU of 8 cores each and a total RAM of 32 GB. When short range emitters are used and mean doses needed, DVK methods, or calculations with specific absorbed fractions, are certainly sufficient. However, when tissue heterogeneities are present, or when emitters have penetrating radiations in their spectrum (e.g., 166Ho), it might be interesting to dispose of Monte-Carlo calculations to assess doses or dose volume histograms. Finally, strategies to limit the computation time of Monte-Carlo calculation can be implemented: limitation of the geometric space and decrease in the spatial resolution.

4.4.3. A workflow for patient-specific dosimetry

Despite the limitations discussed above OEDIPE integrates the essential steps needed to assess patient specific dosimetry. All images used in nuclear medicine can be handled

including combination of SPECT/CT and planar images, in that case the registration and quantification can be performed on any of the SPECT/CT image. Calibration factors can be entered by the user, they can take into account dead time correction, or any correction effect in fact. Moreover, recovery factor can be taken into account independently of this correction factor and all quantification is performed at the VOI level, enabling to use VOI-specific quantification. The biokinetic module integrates several predefined fit functions and if they were not suitable for the user data could be fitted with other programs.

The dosimetry is then assisted by Monte-Carlo calculations, resulting in a workflow that integrates the essential steps for patient-specific dosimetry, avoiding the use of different software along the process.

5. Conclusion

To account for the patient-specific biokinetics, after administration of radiopharmaceuticals, in the estimation of absorbed doses to lesions and healthy tissues, new features were implemented in OEDIPE. These developments enable an automatic analysis of multiple SPECT images or hybrid planar/SPECT images, and to derive the cumulated activity for each VOI. The implemented functionalities have been validated using images acquired with a Jaszczak phantom for both approaches. OEDIPE can now handle 3D Monte Carlo personalized dosimetry including patient-specific anatomy and biokinetics for 246 radionuclides included in the ICRP database. In this work, the implemented features have been applied to a clinical case. When mean absorbed doses are needed, for example to establish dose effect-relationship of small tumours, OEDIPE could be used as a complementary and free tool in clinical trials. OEDIPE can be obtained from IRSN under collaboration agreement. Finally, it

was shown on the studied patient case that the biokinetics of lungs and tumour was consistent with external dose rate measurements and data from the literature. It opens the way for further testing the usefulness of external dose rate measurements as a complementary tool to perform personalized dosimetry.

Acknowledgments

MERAIODE was financed by the French Ministry of Health, through the National Institute for Cancer (INCA, PHRC2015). Dabrafenib and Trametinib were provided by Novartis, rhTSH was provided by Sanofi Genzyme.

IRSN funded the work carried out by its researchers.

Competing interests

Authors declare non conflicts of interest.

References

[1] Beierwaltes WH, Rabbani R, Dmuchowski C, Lloyd RV, Eyre P, Mallette S. An analysis of "ablation of thyroid remnants" with I-131 in 511 patients from 1947-1984: experience at University of Michigan. J Nucl Med. 1984;25:1287-93.
[2] Meier DA, Brill DR, Becker DV, Clarke SEM, Silberstein EB, Royal HD, et al. Procedure Guideline for Therapy of Thyroid Disease with 131Iodine. J Nucl Med. 2002;43:856-61.
[3] Verburg FA, Flux G, Giovanella L, van Nostrand D, Muylle K, Luster M. Differentiated thyroid cancer patients potentially benefitting from postoperative I-131 therapy: a review of the literature of the past decade. Eur J Nucl Med Mol Imaging. 2020;47:78-83. https://doi.org/10.1007/s00259-019-04479-1.
[4] Sgouros G, Bodei L, McDevitt MR, Nedrow JR. Radiopharmaceutical therapy in cancer: clinical advances and challenges. Nat Rev Drug Discov. 2020;19:589-608. https://doi.org/10.1038/s41573-020-0073-9.
[5] Cremonesi M, Ferrari ME, Bodei L, Chiesa C, Sarnelli A, Garibaldi C, et al. Correlation of dose with toxicity and tumour response to (90)Y- and (177)Lu-PRRT provides the basis for optimization through individualized treatment planning. Eur J Nucl Med Mol Imaging. 2018;45:2426-41. https://doi.org/10.1007/s00259-018-4044-x.
[6] Konijnenberg M, Herrmann K, Kobe C, Verburg F, Hindorf C, Hustinx R, et al. EANM position paper on article 56 of the Council Directive 2013/59/Euratom (basic safety standards) for nuclear medicine therapy. Eur J Nucl Med Mol Imaging. 2021;48:67-72. https://doi.org/10.1007/s00259-020-05038-9.
[7] Council of the European Union. European Council Directive 2013/59/EURATOM of 5 December 2013 laying down basic safety standards for protection against the dangers arising from exposure to ionising radiation, and repealing Directives 89/618/Euratom, 90/641/Euratom, 96/29/Euratom, 97/43/Euratom and 2003/122/Euratom. Official Journal of the European Union; 2013.

[8] Siegel JA, Thomas SR, Stubbs JB, Stabin MG. MIRD pamphlet no. 16: techniques for quantitative radiopharmaceutical biodistribution data acquisition and analysis for use in human radiation dose estimates. J Nucl Med. 1999;40:37S.
[9] Garkavij M, Nickel M, Sjogreen-Gleisner K, Ljungberg M, Ohlsson T, Wingardh K, et al. 177Lu-[DOTA0,Tyr3] octreotate therapy in patients with disseminated neuroendocrine tumors: Analysis of dosimetry with impact on future therapeutic strategy. Cancer. 2010;116:1084-92. https://doi.org/10.1002/cncr.24796.
[10] Koral KF, Dewaraja Y, Li J, Barrett CL, Regan DD, Zasadny KR, et al. Initial results for hybrid SPECT-conjugate-view tumor dosimetry in 131I-anti-B1 antibody therapy of previously untreated patients with lymphoma. J Nucl Med. 2000;41:1579-86.
[11] Siegel JA, Thomas SR, Stubbs JB, Stabin MG, Hays MT, Koral KF, et al. MIRD pamphlet no. 16: Techniques for quantitative radiopharmaceutical biodistribution data acquisition and analysis for use in human radiation dose estimates. J Nucl Med. 1999;40:37S-61S.
[12] Capala J, Graves SA, Scott A, Sgouros G, James SS, Zanzonico P, et al. Dosimetry for Radiopharmaceutical Therapy: Current Practices and Commercial Resources. J Nucl Med. 2021;62:3S-11S. https://doi.org/10.2967/jnumed.121.262749.
[13] Kayal G, Clayton N, Vergara-Gil A, Struelens L, Bardiès M. Proof-of-concept of DosiTest: A virtual multicentric clinical trial for assessing uncertainties in molecular radiotherapy dosimetry. Phys Med. 2022;97:25-35. https://doi.org/https://doi.org/10.1016/j.ejmp.2022.03.011.
[14] Stabin MG, Sparks RB, Crowe E. OLINDA/EXM: The Second-Generation Personal Computer Software for Internal Dose Assessment in Nuclear Medicine. J Nucl Med. 2005;46:1023-7.
[15] Dieudonne A, Hobbs RF, Bolch WE, Sgouros G, Gardin I. Fine-resolution voxel S values for constructing absorbed dose distributions at variable voxel size. J Nucl Med. 2010;51:1600-7. https://doi.org/10.2967/jnumed.110.077149.
[16] Shiiba T, Kuga N, Kuroiwa Y, Sato T. Evaluation of the accuracy of mono-energetic electron and beta-emitting isotope dose-point kernels using particle and heavy ion transport code system: PHITS. Appl Radiat Isot. 2017;128:199-203. https://doi.org/10.1016/j.apradiso.2017.07.028.
[17] Götz T, Schmidkonz C, Lang EW, Maier A, Kuwert T, Ritt P. A comparison of methods for adapting ^{177}Lu dose-voxel-kernels to tissue inhomogeneities. Phys Med Biol. 2019;64:245011. https://doi.org/10.1088/1361-6560/ab5b81.
[18] Dieudonne A, Hobbs RF, Lebtahi R, Maurel F, Baechler S, Wahl RL, et al. Study of the impact of tissue density heterogeneities on 3-dimensional abdominal dosimetry: comparison between dose kernel convolution and direct Monte Carlo methods. J Nucl Med. 2013;54:236-43. https://doi.org/10.2967/jnumed.112.105825.
[19] Bolch WE, Bouchet LG, Robertson JS, Wessels BW, Siegel JA, Howell RW, et al. MIRD pamphlet no. 17: The dosimetry of nonuniform activity distributions - Radionuclide S values at the voxel level. J Nucl Med. 1999;40:11S-36S.
[20] Amato E, Auditore L, Italiano A, Pistone D, Arce P, Campennì A, et al. Full Monte Carlo internal dosimetry in nuclear medicine by means of GAMOS. J Phys Conf Ser. 2020;1561:012002. https://doi.org/10.1088/1742-6596/1561/1/012002.
[21] Sato T, Furuta T, Liu Y, Naka S, Nagamori S, Kanai Y, et al. Individual dosimetry system for targeted alpha therapy based on PHITS coupled with microdosimetric kinetic model. EJNMMI Phys. 2021;8:4. https://doi.org/10.1186/s40658-020-00350-7.
[22] Mora-Ramirez E, Santoro L, Cassol E, Ocampo-Ramos JC, Clayton N, Kayal G, et al. Comparison of commercial dosimetric software platforms in patients treated with (177) Lu-DOTATATE for peptide receptor radionuclide therapy. Med Phys. 2020;47:4602-15. https://doi.org/10.1002/mp.14375.
[23] Della Gala G, Bardiès M, Tipping J, Strigari L. Overview of commercial treatment planning systems for targeted radionuclide therapy. Phys Med. 2021;92:52-61. https://doi.org/https://doi.org/10.1016/j.ejmp.2021.11.001.
[24] Grassi E, Fioroni F, Ferri V, Mezzenga E, Sarti MA, Paulus T, et al. Quantitative comparison between the commercial software STRATOS(®) by Philips and a homemade software for voxel-

dosimetry in radiopeptide therapy. Phys Med. 2015;31:72-9.
https://doi.org/10.1016/j.ejmp.2014.10.002.
[25] Kafrouni M, Allimant C, Fourcade M, Vauclin S, Delicque J, Ilonca AD, et al. Retrospective Voxel-Based Dosimetry for Assessing the Ability of the Body-Surface-Area Model to Predict Delivered Dose and Radioembolization Outcome. J Nucl Med. 2018;59:1289-95.
https://doi.org/10.2967/jnumed.117.202937.
[26] Rosar F, Schön N, Bohnenberger H, Bartholomä M, Stemler T, Maus S, et al. Comparison of different methods for post-therapeutic dosimetry in [(177)Lu]Lu-PSMA-617 radioligand therapy. EJNMMI Phys. 2021;8:40. https://doi.org/10.1186/s40658-021-00385-4.
[27] Andersson M, Johansson L, Eckerman K, Mattsson S. IDAC-Dose 2.1, an internal dosimetry program for diagnostic nuclear medicine based on the ICRP adult reference voxel phantoms. EJNMMI Res. 2017;7:88. https://doi.org/10.1186/s13550-017-0339-3.
[28] Wahl RL, Frey EC, Jacene HA, Kahl BS, Piantadosi S, Bianco JA, et al. Prospective SPECT-CT Organ Dosimetry-Driven Radiation-Absorbed Dose Escalation Using the In-111 ((111)In)/Yttrium 90 ((90)Y) Ibritumomab Tiuxetan (Zevalin(®)) Theranostic Pair in Patients with Lymphoma at Myeloablative Dose Levels. Cancers. 2021;13. https://doi.org/10.3390/cancers13112828.
[29] Hagmarker L, Svensson J, Rydén T, van Essen M, Sundlöv A, Gleisner KS, et al. Bone Marrow Absorbed Doses and Correlations with Hematologic Response During (177)Lu-DOTATATE Treatments Are Influenced by Image-Based Dosimetry Method and Presence of Skeletal Metastases. J Nucl Med. 2019;60:1406-13. https://doi.org/10.2967/jnumed.118.225235.
[30] Kupitz D, Wetz C, Wissel H, Wedel F, Apostolova I, Wallbaum T, et al. Software-assisted dosimetry in peptide receptor radionuclide therapy with 177Lutetium-DOTATATE for various imaging scenarios. PloS one. 2017;12:e0187570. https://doi.org/10.1371/journal.pone.0187570.
[31] Chiavassa S, Aubineau-Laniece I, Bitar A, Lisbona A, Barbet J, Franck D, et al. Validation of a personalized dosimetric evaluation tool (Oedipe) for targeted radiotherapy based on the Monte Carlo MCNPX code. Phys Med Biol. 2006;51:601-16. https://doi.org/10.1088/0031-9155/51/3/009.
[32] Petitguillaume A, Bernardini M, Broggio D, De Labriolle Vaylet C, Franck D, Desbreé A. OEDIPE, a software for personalized Monte Carlo dosimetry and treatment planning optimization in nuclear medicine: Absorbed dose and biologically effective dose considerations. Radioprotection. 2014;49:275-81. https://doi.org/10.1051/radiopro/2014021.
[33] Benabdallah N. Optimisation de la dosimétrie en alphathérapie par approche multi-échelle : application au traitement des métastases osseuses par le ^{223}Ra (Optimization of dosimetry in alphatherapy by a multi-scale approach : application to the treatment of bone metastases with ^{223}Ra): Thesis, Université Paris-Saclay; 2017.
[34] Finocchiaro D, Gear JI, Fioroni F, Flux GD, Murray I, Castellani G, et al. Uncertainty analysis of tumour absorbed dose calculations in molecular radiotherapy. EJNMMI Phys. 2020;7:63.
https://doi.org/10.1186/s40658-020-00328-5.
[35] Ilan E, Sandström M, Wassberg C, Sundin A, Garske-Román U, Eriksson B, et al. Dose response of pancreatic neuroendocrine tumors treated with peptide receptor radionuclide therapy using 177Lu-DOTATATE. J Nucl Med. 2015;56:177-82. https://doi.org/10.2967/jnumed.114.148437.
[36] International Commission on Radiological Protection. Radionuclide Transformations - Energy and Intensity of Emissions. ICRP Publication 38. 1983;Ann. ICRP 11-13.
[37] Hendricks JS, McKinney GW, Fensin ML, James MR, Johns RC, Durkee JW, et al. MCNPX 2.6.0 Extensions [LA-UR-08-2216].Los Alamos: Los Alamos National Laboratory; 2008.
[38] Gregory RA, Murray I, Gear J, Leek F, Chittenden S, Fenwick A, et al. Standardised quantitative radioiodine SPECT/CT Imaging for multicentre dosimetry trials in molecular radiotherapy. Phys Med Biol. 2019;64:245013. https://doi.org/10.1088/1361-6560/ab5b6c.
[39] Erlandsson K, Buvat I, Pretorius PH, Thomas BA, Hutton BF. A review of partial volume correction techniques for emission tomography and their applications in neurology, cardiology and oncology. Phys Med Biol. 2012;57:R119-59. https://doi.org/10.1088/0031-9155/57/21/R119.
[40] Leboulleux S, Cao CD, Zerdoud S, Attard M, Bournaud C, Benisvy D, et al. MERAIODE: A Redifferentiation Phase II Trial With Trametinib and Dabrafenib Followed by Radioactive Iodine

Administration for Metastatic Radioactive Iodine Refractory Differentiated Thyroid Cancer Patients With a BRAFV600E Mutation (NCT 03244956). J Endocr Soc. 2021;5:A876-A. https://doi.org/10.1210/jendso/bvab048.1789.
[41] International Commission on Radiation Units & Measurements. ICRU Report 44: Tissue Substitutes in Radiation Dosimetry and Measurement 1989.
[42] van Gils CAJ, Beijst C, van Rooij R, de Jong HWAM. Impact of reconstruction parameters on quantitative I-131 SPECT. Phys Med Biol. 2016;61:5166-82. https://doi.org/10.1088/0031-9155/61/14/5166.
[43] Dewaraja YK, Ljungberg M, Green AJ, Zanzonico PB, Frey EC, Bolch WE, et al. MIRD pamphlet No. 24: Guidelines for quantitative 131I SPECT in dosimetry applications. J Nucl Med. 2013;54:2182-8. https://doi.org/10.2967/jnumed.113.122390.
[44] Dewaraja YK, Frey EC, Sgouros G, Brill AB, Roberson P, Zanzonico PB, et al. MIRD pamphlet No. 23: quantitative SPECT for patient-specific 3-dimensional dosimetry in internal radionuclide therapy. J Nucl Med. 2012;53:1310-25. https://doi.org/10.2967/jnumed.111.100123.
[45] Verburg FA, Hänscheid H, Luster M. Radioactive iodine (RAI) therapy for metastatic differentiated thyroid cancer. Best Pract Res Clin Endocrinol Metab. 2017;31:279-90. https://doi.org/10.1016/j.beem.2017.04.010.
[46] Rani D, Kaisar S, Awasare S, Kamaldeep, Abhyankar A, Basu S. Examining recombinant human TSH primed ^{131}I therapy protocol in patients with metastatic differentiated thyroid carcinoma: comparison with the traditional thyroid hormone withdrawal protocol. Eur J Nucl Med Mol Imaging. 2014;41:1767-80. https://doi.org/10.1007/s00259-014-2737-3.
[47] Pötzi C, Moameni A, Karanikas G, Preitfellner J, Becherer A, Pirich C, et al. Comparison of iodine uptake in tumour and nontumour tissue under thyroid hormone deprivation and with recombinant human thyrotropin in thyroid cancer patients. Clin Endocrinol. 2006;65:519-23. https://doi.org/10.1111/j.1365-2265.2006.02626.x.
[48] de Keizer B, Brans B, Hoekstra A, Zelissen PM, Koppeschaar HP, Lips CJ, et al. Tumour dosimetry and response in patients with metastatic differentiated thyroid cancer using recombinant human thyrotropin before radioiodine therapy. Eur J Nucl Med Mol Imaging. 2003;30:367-73. https://doi.org/10.1007/s00259-002-1076-y.
[49] Hänscheid H, Lassmann M, Luster M, Thomas SR, Pacini F, Ceccarelli C, et al. Iodine biokinetics and dosimetry in radioiodine therapy of thyroid cancer: procedures and results of a prospective international controlled study of ablation after rhTSH or hormone withdrawal. J Nucl Med. 2006;47:648-54.
[50] Remy H, Borget I, Leboulleux S, Guilabert N, Lavielle F, Garsi J, et al. 131I effective half-life and dosimetry in thyroid cancer patients. J Nucl Med. 2008;49:1445-50. https://doi.org/10.2967/jnumed.108.052464.
[51] Wierts R, Brans B, Havekes B, Kemerink GJ, Halders SG, Schaper NN, et al. Dose-Response Relationship in Differentiated Thyroid Cancer Patients Undergoing Radioiodine Treatment Assessed by Means of 124I PET/CT. J Nucl Med. 2016;57:1027-32. https://doi.org/10.2967/jnumed.115.168799.
[52] Song H, He B, Prideaux A, Du Y, Frey E, Kasecamp W, et al. Lung dosimetry for radioiodine treatment planning in the case of diffuse lung metastases. J Nucl Med. 2006;47:1985-94.
[53] Sgouros G, Kolbert KS, Sheikh A, Pentlow KS, Mun EF, Barth A, et al. Patient-specific dosimetry for 131I thyroid cancer therapy using 124I PET and 3-dimensional-internal dosimetry (3D-ID) software. J Nucl Med. 2004;45:1366-72.
[54] Klain M, Nappi C, De Risi M, Piscopo L, Volpe F, Manganelli M, et al. Whole-Body Radioiodine Effective Half-Life in Patients with Differentiated Thyroid Cancer. Diagnostics. 2021;11:1740. https://doi.org/10.3390/diagnostics11101740.

List of abbreviations

OEDIPE: Outil d'Evaluation de la Dose Interne Personnalisée (Numerical tool for the personalized assessment of internal dose)

CT: Computed tomography

DICOM: Digital Imaging and Communications in Medicine

DVK: the convolution of dose voxel kernels

MCNPX: Monte-Carlo N-Particle transport code

MIRD: Medical internal radiation dose

NM: Nuclear medicine

SPECT: Single-photon emission computed tomography

TACs: time-activity curves

TEP: positron emission tomography

VOI: Volume of interest

WB: whole body

List of figure captions

Figure 1. Flowchart of OEDIPE modules enabling calculation of a personalized 3D dose from anatomical and functional data of the patient. New implementations are represented by blue boxes.

Figure 2. Planar registration interface enabling registration of the SPECT projections onto the anterior and posterior views of the planar image.

Figure 3. Coronal (A) and transverse (B) slices of the SPECT/CT image of the patient. Anterior (C) and posterior (D) planar scintigraphies of the patient acquired before the SPECT/CT. The lesions are labelled as in the main text.

Figure 4. Time-activity curves in I-131 for three spheres of the **Jaszczak** phantom: comparison of the results obtained with OEDIPE using the multi-SPECT approach with the known values

Figure 5. Comparison of cumulated activities obtained from the multi-SPECT (left) and planar-SPECT approaches (right) with theoretical ones (value of 100%). For the planar-SPECT approach, each of the six series of data corresponds to the association of the planar images with a SPECT image acquired at a different time among the six available.

Figure 6. Comparison of the time-activity data points for I-131 in three **Jaszczak** phantom spheres, obtained from the six image associations (Planar + SPECT_i, i varied from 1 to 6), with the theoretical curves.

Figure 7. Time-Activity Curves (TACs) of different VOIs of the patient resulting from OEDIPE Planar-SPECT approach (in blue) and from SPECT data combining whole-body effective half-life (WB-SPECT approach, in green)

Supplementary Material

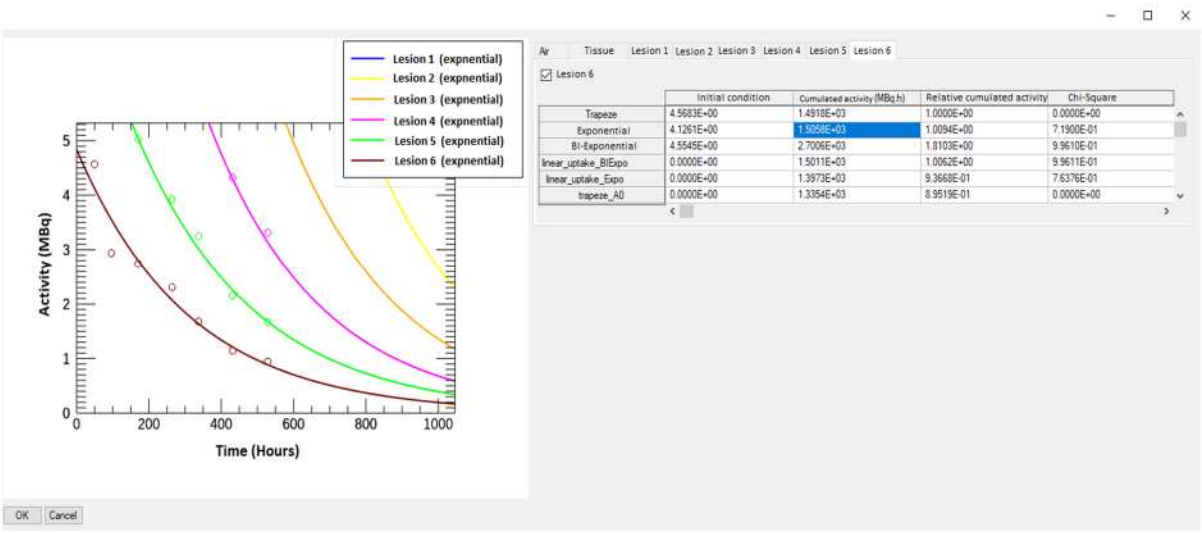

Figure S.1 Screen capture of the Biokinetics module. Right: the display of the TACs curves of the volumes of interest (VOIs). Left: the different fit functions available for each VOI, and the useful information for each function choice (cumulated activity, initial condition, chi-square).

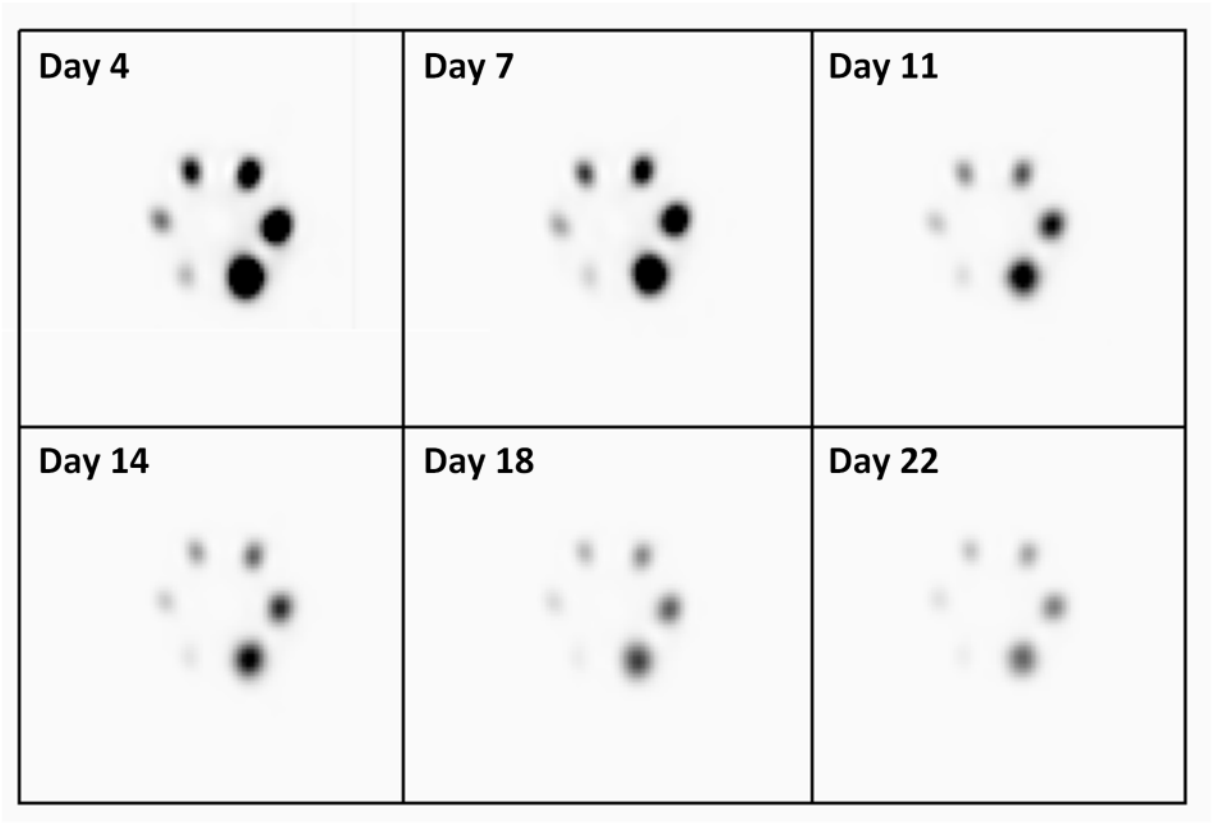

Figure S.2 Axial views of the six SPECT acquisitions of the Jaszczak phantom used to validate the image analysis processes implemented in OEDIPE to derive time-activity data.

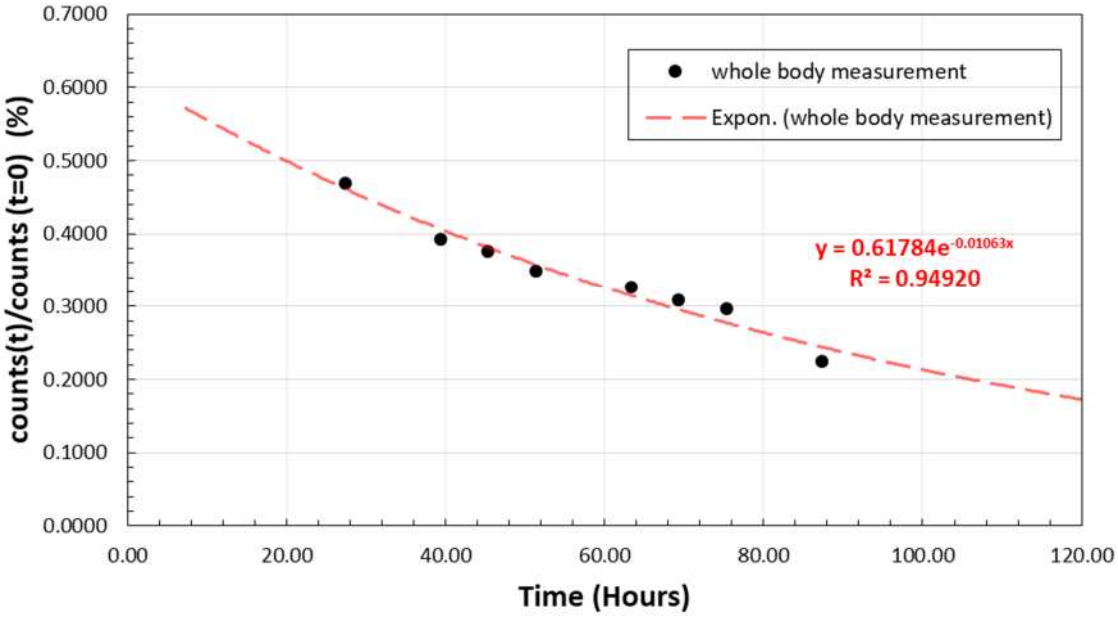

Figure S.3 Whole-body measurements of the patient after treatment with I-131 and corresponding fitting curve. Measurement data were normalized using the measurement result obtained right after I-131 administration.

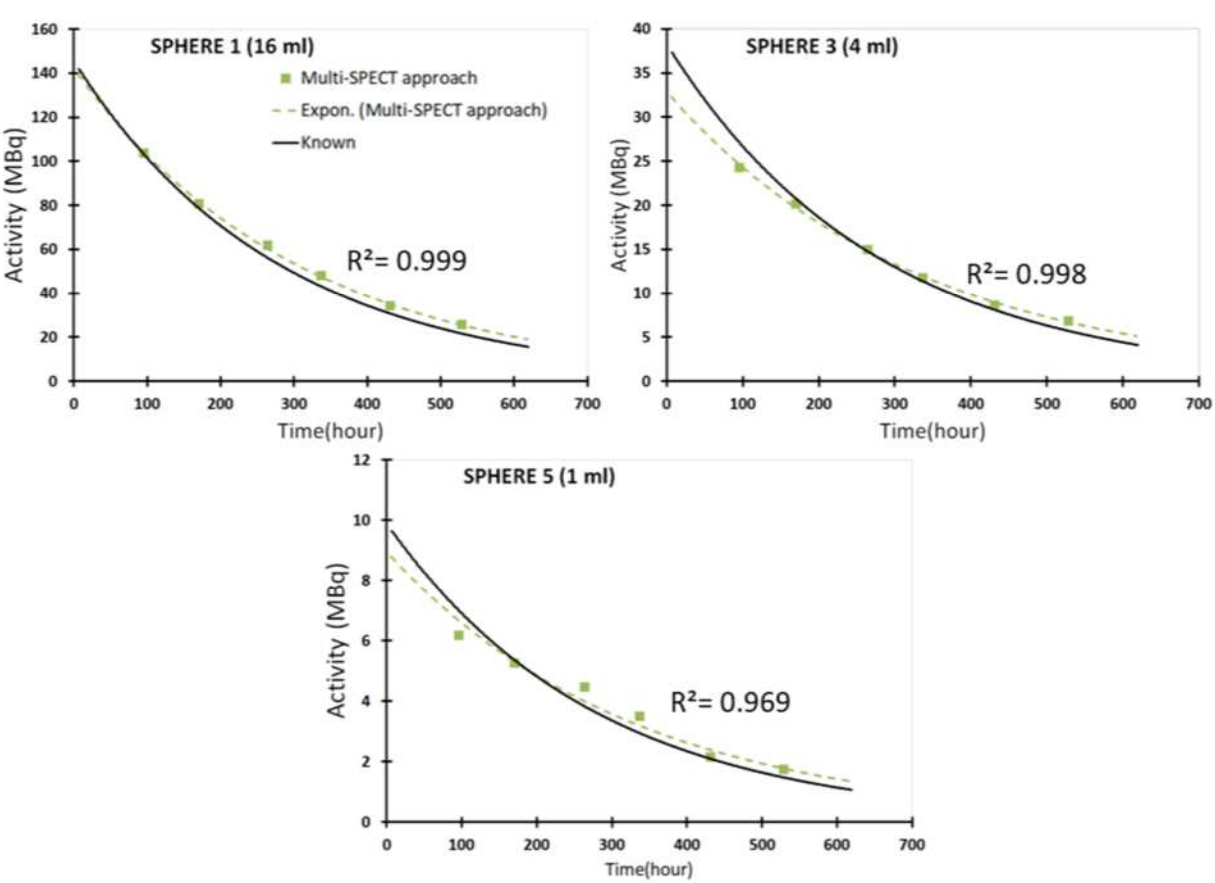

Figure S.4 Time-activity curves in I-131 for three spheres of the Jaszczak phantom: comparison of the results obtained with OEDIPE using the multi-SPECT approach with the known values

Table S.1 Recovery coefficient used to derive activity in the Jaszczak phantom spheres and associated time-activity curve (TAC) characteristics (r-squared value of the fit, effective half-life and cumulated activity).

Sphere	Volume (mL)	Recovery coefficient	R-squared value of the fitting TAC	Effective half-life (h)	Cumulated activity (MBq.h)
Sphere 1	16	0.760	0.999	213.3	40144.6
Sphere 2	8	0.657	0.0997	215.3	22860.7
Sphere 3	4	0.481	0.998	230.3	10921.7
Sphere 4	2	0.344	0.986	239.8	5783.7
Sphere 5	1	0.151	0.969	226.5	2922.9
Sphere 6	0.5	0.074	0.959	240.7	1463.4

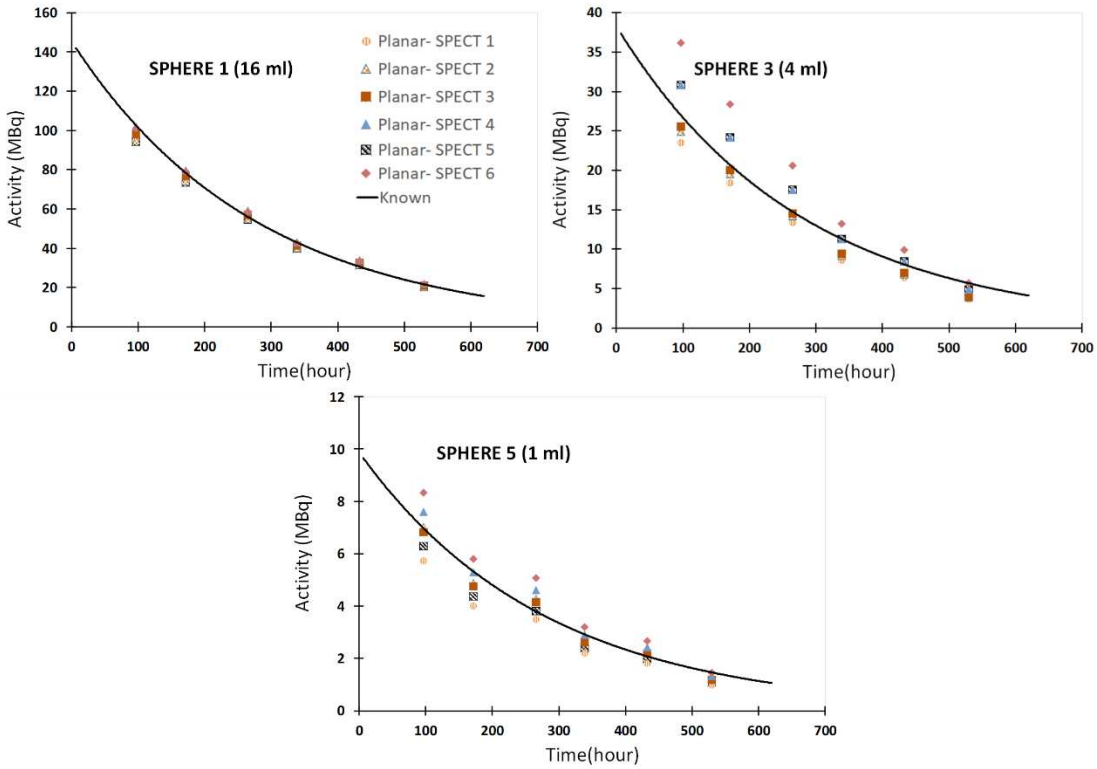

Figure S.5 Comparison of the time-activity data points for I-131 in three **Jaszczak** phantom spheres, obtained from the six image associations (Planar + SPECT_i, i varied from 1 to 6), with the theoretical curves.